Electron Scattering from ^{19}F and ^{40}Ca†

P. L. Hallowell,* W. Bertozzi, J. Heisenberg, S. Kowalski, X. Maruyama,‡
C. P. Sargent, W. Turchinetz, and C. F. Williamson
Laboratory for Nuclear Science and Department of Physics, Massachusetts Institute of Technology, Cambridge, Massachusetts 02139

and

S. P. Fivozinsky, J. W. Lightbody, Jr.,§ and S. Penner
National Bureau of Standards, Washington, D. C. 20234

(Received 25 October 1972)

Electron scattering form factors were measured for the low-lying levels of ^{19}F and ^{40}Ca for momentum transfers between 0.55 and 1.00 fm^{-1}. Elastic scattering from ^{19}F yields an rms charge radius of 2.885± 0.015 fm. Transition strengths and transition radii are obtained for the lowest $\frac{5}{2}^+$, $\frac{5}{2}^-$, and $\frac{3}{2}^+$ states in ^{19}F. A deformed rotational model gives a very good fit to the form factors for the positive-parity levels with ground-state deformation parameters of $\beta_2 = 0.41$ and $\beta_4 = 0.17$. The form factors for excitation of the 3^- and 2^+ states in ^{40}Ca are analyzed by phase-shift analysis, and transition strengths and transition radii are also obtained for these levels.

INTRODUCTION

This paper presents form factors for elastic and inelastic electron scattering from ^{19}F and inelastic electron scattering from ^{40}Ca. These two nuclei are quite different in structure. They were studied together mainly because they occur together in the form of CaF_2, a chemical compound whose physical properties are suitable for fabricating a good electron scattering target. This turns out to be a fortunate circumstance experimentally because very accurate elastic electron scattering form factors are available for ^{40}Ca. Thus, the target contains a built-in normalization for all the measured form factors.

The low-lying level structure of ^{19}F is indicated schematically in Fig. 1(a), while the same information is given for ^{40}Ca in Fig. 1(b). In the case of ^{19}F the $\frac{1}{2}^+$ [ground state (g.s.)], the $\frac{5}{2}^+$ (0.197-MeV), the $\frac{5}{2}^-$ (1.346-MeV), and the $\frac{3}{2}^+$ (1.554-MeV) levels were studied. The $E1$ transitions to the $\frac{1}{2}^-$ (0.110-MeV) and the $\frac{3}{2}^-$ (1.459-MeV) levels were too weak to be seen in the present experiment. In the case of ^{40}Ca the 3^- (3.737-MeV) and the 2^+ (3.904-MeV) levels were studied. The $E0$ transition to the 0^+ (3.354-MeV) state was not observed.

Electron scattering form factors were measured for the observed levels in the momentum transfer range from about 0.55 to 1.0 fm^{-1} at three different laboratory scattering angles. The form factors were extrapolated to zero momentum transfer to obtain the transition strengths for the various levels.

PREVIOUS EXPERIMENTAL WORK

^{19}F

The electromagnetic transition strengths for the low-lying levels of ^{19}F have been measured in a number of experiments. Poletti, Becker, and McDonald[1] using the (p, p') reaction and the Doppler-shift attenuation method have determined excitation energies, lifetimes, and branching ratios for the $\frac{5}{2}^-$ (1.346-MeV) level, the $\frac{3}{2}^-$ (1.459-MeV) level, and the $\frac{3}{2}^+$ (1.554-MeV) level. The lifetime of the $\frac{5}{2}^+$ (0.197-MeV) level has been measured by Becker, Olness, and Wilkinson.[2] Coulomb excitation of the low-lying ^{19}F levels has been studied by Stelson and McGowan,[3] by Litherland, Clark, and Broude,[4] and by Alexander *et al.*[5] Electron scattering to the 1.346- and 1.554-MeV states was observed by Walcher and Strehl[6] at incident energies of 36 and 58 MeV. Excitation strengths of the various levels in ^{19}F have also been derived from proton[7,8] and deuteron[9] scattering experiments.

^{40}Ca

In the present experiment the form factors were measured only for the 3^- (3.737-MeV) and 2^+ (3.904-MeV) levels. Electromagnetic transition strengths have been measured for these levels in (p, γ) and $(p, p'\gamma)$ experiments.[10-13] Excitation strengths have also been derived for (α, α') experiments.[14] Inelastic electron scattering from these two levels has been observed by Blum, Barreau, and Bellicard[15] at incident energies between

120 and 220 MeV. Eisenstein *et al.*[16] measured the form factors for exciting the 3^- and 2^+ levels at momentum transfers between 0.34 and 0.57 fm^{-1}. The excitation strengths of these two levels were also measured by Strehl[17] in inelastic electron scattering at a momentum transfer of 0.46 fm^{-1}. Higher-energy inelastic electron scattering experiments were carried out by Itoh, Oyamada, and Torizuka[18] and by Heisenberg, McCarthy, and Sick[19] for momentum transfers between 0.6 and 2.4 fm^{-1}. In the latter two experiments an experimental separation of the levels was not possible.

EXPERIMENTAL ARRANGEMENT AND DATA ACQUISITION

Only a brief description will be given here of the experimental arrangement, since the National Bureau of Standards electron linear accelerator[20] and the associated beam transport system and high-resolution spectrometer[21] have been described in detail elsewhere. This facility is capable of producing electron beams up to 5-μA intensity at energies up to 120 MeV with an over-all experimental resolution better than 0.1%.

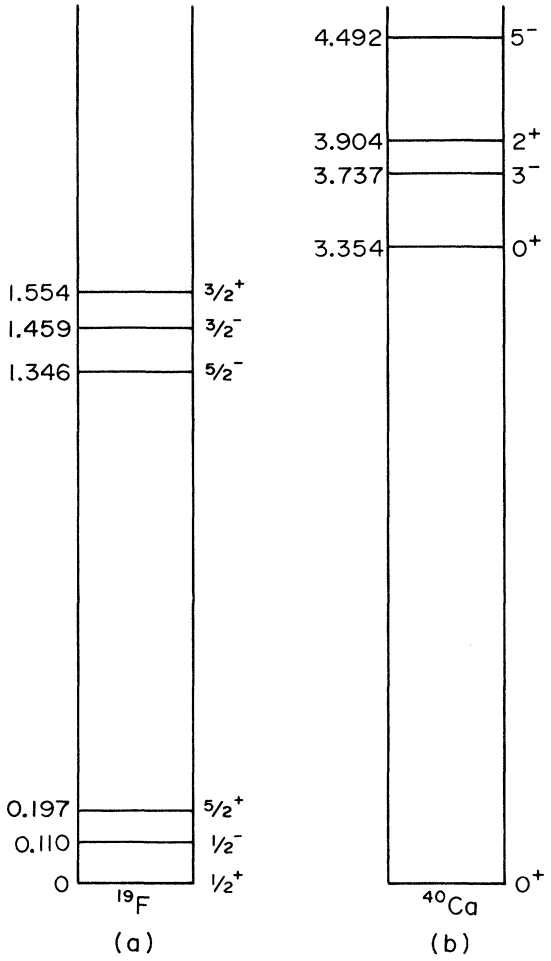

FIG. 1. Schematic diagram of the low-lying states in ^{19}F and ^{40}Ca.

The targets used in this experiment were optical grade crystals of CaF_2. The beam from the accelerator was energy analyzed and focused on the target as an achromatic spot approximately 1 mm high × 1 mm wide. The transmitted current was collected and integrated by a Faraday cup whose absolute charge collection efficiency is known to 0.1%. At the lower energies the multiple scattering in the target caused an appreciable fraction of the beam to be scattered outside the acceptance cone of the Faraday cup. However, since all cross sections in this experiment were measured relative to the calcium elastic cross sections, the loss of the beam from the Faraday cup was unimportant. In addition to the Faraday cup, a nonintercepting ferrite transformer[22] was used as a secondary beam current monitor. This ferrite monitor was calibrated with respect to the Faraday cup at frequent intervals.

For all runs except those at 163° the targets were oriented in the beam in the "transmission" mode so that the normal to the target surface bisected the scattering angle. Under these conditions the mean energy loss in the target does not contribute to the experimental peak width. For the 163° scattering runs the targets could not be mounted in the transmission mode. Instead, the target was mounted so that a line parallel to the surface bisected the scattering angle. In this "reflection" mode, the scattered electron energy distribution was somewhat broadened due to energy loss in the target.

The spectrometer was an $n = \frac{1}{2}$ double-focusing 169.8° magnet with a mean particle radius of curvature of 0.762 m, accepting a solid angle of approximately 4.9 msr. The absolute calibration was known to one part in 10^3, and the relative calibration was accurate to one part in 10^4. The scattered electrons were detected at the focal plane of the spectrometer by a "ladder" array of 20 lithium-drifted silicon detectors. This array was mounted on a movable frame whose position was controlled by a precision stepping motor. In tandem behind the semiconductor detectors were two plastic scintillators whose purpose was to discriminate background counts from real electron scattering events.

All information was fed to an on-line XDS-920 computer. The computer provided a live display of the scattered electron spectra, control of the experiment, and a record on magnetic tape of the experimental data and parameters.

DATA REDUCTION

Counting Loss and Efficiency Corrections

The largest counting loss correction to the data was due to an electronic restriction of one count per beam pulse per semiconductor detector. The corrections for this counting loss have been worked out in detail[23] and were applied to the present data. Corrections were also made for the dead time of the photomultiplier discriminators, and for the accidental coincidences between semiconductor singles and photomultiplier double coincidences. The correction due to the one-count-per-beam-burst restriction was never greater than 10%, and the other corrections were of the order of 2–4%. The relative efficiencies of the detectors in the focal plane array were determined by observing the corrected counts per unit beam charge for different detectors viewing the same portion of the spectrum.

Line-Shape Fitting

The observed spectrum of inelastic levels was superimposed on a continuous background. This background was composed primarily of the radiative tails of the elastic peaks and of the inelastic peaks at lower excitation. In addition there was also a small background due to room radiation.

The magnitude of the room background was estimated by observing the background at spectrometer magnetic fields corresponding to momenta larger than that of the ^{40}Ca elastic peak. It was assumed that the room radiation background was constant as a function of spectrometer field. This constant background was subtracted before beginning the line-shape analysis.

Two methods were used for subtracting the radiation tails:

(i) For the ^{40}Ca levels, which were located near 4 MeV excitation, the background was smooth; and it was found that for limited regions on each side of the inelastic peaks this background could be represented by a linear function.

(ii) For the ^{19}F levels, which were at excitation energies less than 1.6 MeV, it was necessary to calculate the elastic radiation tail. This was done by computer using the formalism of Nguyen-Ngoc and Perez-y-Jorba.[24] The calculated elastic radiation tail was normalized to fit the observed elastic radiation tail at momenta greater than that of the first inelastic peak. This elastic radiation tail was then subtracted from the spectrum, leaving only the inelastic peaks.

The areas of the peaks in the resulting inelastic spectrum were then extracted. This was accomplished using a nonlinear least-squares computer code that reproduced the line shape by a convolution of the Landau line shape[25] due to energy loss in the target, the Schwinger[26] radiation due to nuclear scattering, the non-nuclear bremsstrahlung, and an empirical function representing the experimental resolution function. The latter was assumed to have a Gaussian shape. The fixed parameters in the calculation were the incident energy, the scattering angle, and the target thickness and composition. The variable parameters were the position and relative height of each peak and the width of the Gaussian function representing the instrumental resolution. These parameters were varied to obtain a minimum least-squares fit to the inelastic spectrum. The subtraction and fitting procedures are illustrated with actual spectra in Figs. 2(a)–2(d).

All nonlinear least-squares fitting in the present work was accomplished using an iterative method. This procedure consisted of linearization of the fitting function by expanding it in a Taylor's series in the parameters and retaining only the terms through the first derivatives. The goodness of fit of the function to the experimental data was measured by the familiar χ^2 test. The quoted errors for the fitted parameters are correlated errors and represent the maximum variation possible for each parameter consistent with an increase of χ^2 by one unit.

Extraction of the Relative Form Factors

The differential scattering cross section can be expressed in the form

$$\frac{d\sigma}{d\Omega} = \left(\frac{d\sigma}{d\Omega}\right)_0 |F(q)|^2 \eta^{-1}, \tag{1a}$$

where

$$\left(\frac{d\sigma}{d\Omega}\right)_0 = 10\left(\frac{\alpha^2 Z^2}{4K_0^2}\right)\cos^2(\tfrac{1}{2}\theta)\csc^4(\tfrac{1}{2}\theta) \tag{1b}$$

is the Mott scattering cross section in mb/sr for an infinitely massive point charge and

$$\eta = 1 + (2E_0/M)\sin^2(\tfrac{1}{2}\theta) \tag{1c}$$

is the kinematic recoil factor. The momentum transfer, $q(\mathrm{fm}^{-1})$, is given by

$$q = 2K_0\eta^{-1}(1-\omega/E_0)^{1/2}\sin\tfrac{1}{2}\theta. \tag{1d}$$

It is sometimes convenient to use the "effective" or "local" momentum transfer defined as

$$q_{\mathrm{eff}} = q\left[1 + (\tfrac{4}{3})\alpha Z/(K_0\langle r^2\rangle^{1/2})\right]. \tag{1e}$$

$F(q)$ is the form factor arising from the fact that the nucleus is not a point charge. The other symbols are defined as follows: $\langle r^2\rangle^{1/2}$ is the rms nuclear ground-state radius (fm), ω is the nuclear excitation energy (MeV), α is the fine-structure

constant, θ is the laboratory scattering angle, Z is the atomic number of target nucleus, M is the mass of target nucleus (MeV), E_0 is the total energy of incident electron (MeV), and $K_0 = E_0/197.32$ (fm^{-1}).

In the present experiment the form factors of each level were compared to the elastic scattering form factor of ^{40}Ca. Thus, the ratios of the bremsstrahlung corrections, the ionization corrections, and the constant factors cancel because all experiments were performed in the same target. The ratio of the Schwinger corrections differs negligibly from unity for this experiment. Thus the ratio of form factors is given by

$$\frac{F_j^2(q)}{F_0^2(q)} = \frac{N_j Z_0^2 \eta_j n_0}{N_0 Z_j^2 \eta_0 n_j}, \tag{2}$$

where n_j is the number of atoms/molecule for

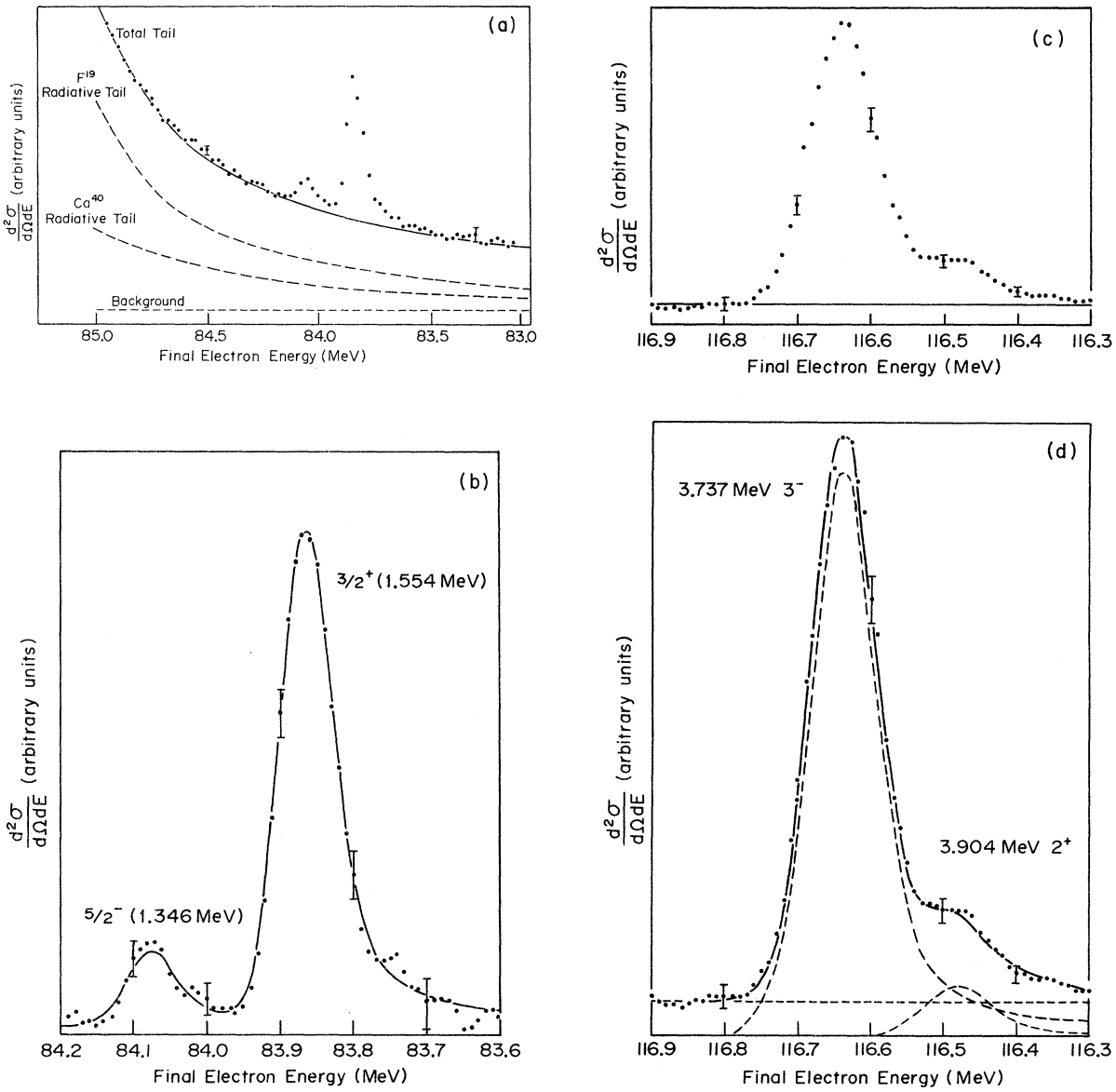

FIG. 2. Illustration of radiative tail subtraction and line-shape fitting for the data. (a) Unsubtracted spectrum for ^{19}F at an incident electron energy of 86.05 MeV and at a laboratory angle of 110.6°. The various backgrounds to be subtracted are indicated. (b) Subtracted spectrum for ^{19}F showing line-shape fitting (solid curve). This is a portion of the same spectrum shown in Fig. 1(a). (c) Unsubtracted spectrum for ^{40}Ca at an incident electron energy of 121.00 MeV and at a laboratory angle of 110.6°. The assumed background is indicated. (d) Subtracted spectrum for ^{40}Ca showing line-shape fitting. This is the same spectrum as in Fig. 1(c).

the jth species, and N_j is the number of counts/charge for the jth species.

Normalization to ^{40}Ca Elastic Scattering

In order to derive the form factor for the ith level using Eq. (2) it is necessary to know $F_0(q)$, the elastic scattering form factors for ^{40}Ca. This was not measured in the present experiment. However, measurements of these quantities have been made by Frosch *et al.*[27] at 250 and 500 MeV, and by Eisenstein *et al.*[16] at 43 and 60 MeV. More recently, unpublished measurements have been made by the Stanford[28] group of the elastic electron scattering form factors for ^{40}Ca.

The data of Eisenstein *et al.*[16] were fitted by a simple Fermi charge distribution of the form

$$\rho(r) = \rho_0(1 + e^{(r-c)/z})^{-1}. \quad (3)$$

The best phase-shift calculation fit to their data yielded the following parameters:

$c = 3.650$ fm,

$z = 0.5188$ fm.

This will subsequently be referred to as model 1.

TABLE I. Calculated elastic electron scattering form factors for ^{40}Ca.

E (MeV) [a]	θ (deg) [b]	q (fm^{-1})	$F(q)$ [c] model 1	model 2	model 3
60.3	70.27	0.352	0.809	0.801	0.802
60.3	90.11	0.432	0.697	0.687	0.688
60.3	110.08	0.500	0.595	0.583	0.584
60.3	128.91	0.551	0.518	0.505	0.506
60.3	150.00	0.589	0.4589	0.4462	0.4463
66.02	110.75	0.550	0.5195	0.5070	0.5075
71.02	110.75	0.592	0.4580	0.4455	0.4455
71.03	110.64	0.591	0.4585	0.4460	0.4460
86.05	110.64	0.716	0.2909	0.2804	0.2790
101.17	110.64	0.842	0.1574	0.1508	0.1483
101.21	110.40	0.841	0.1582	0.1517	0.1491
121.00	110.64	1.006	0.047 54	0.046 08	0.044 09
60.88	145.82	0.589	0.4600	0.4471	0.4471
68.55	145.79	0.663	0.3540	0.3420	0.3412
73.94	145.82	0.715	0.2862	0.2753	0.2738
74.45	145.70	0.720	0.2803	0.2696	0.2681
87.96	145.40	0.849	0.1423	0.1360	0.1334
104.59	145.79	1.011	0.041 50	0.039 59	0.038 32
104.65	145.70	1.011	0.041 41	0.039 49	0.038 24
85.41	163.21	0.855	0.1361	0.1299	0.1273
Parameters		c (fm)	3.650	3.6758	3.7984
		z (fm)	0.5188	0.5851	0.5795
		w (fm)	0.0	−0.1017	−0.1779

[a] Calculations for 60.3 MeV correspond to the data of Ref. 16; other energies correspond to the present data.
[b] Laboratory scattering angle.
[c] Various models discussed in text.

The data of Frosch *et al.*[27] were fitted in a phase-shift calculation using a parabolic Fermi charge distribution of the form

$$\rho(r) = \rho_0(1 + w^2/c^2)(1 + e^{(r-c)/z})^{-1}. \quad (4)$$

The best fit to their data (which also fitted the mu-mesic x-ray energies) yielded the following parameters:

$c = 3.6758$ fm,

$z = 0.5851$ fm,

$w = -0.1017$ fm.

This will subsequently be referred to as model 2.

The unpublished data of the Stanford group[28] were also fitted in a phase-shift analysis (requiring a fit to the mu-mesic x-ray energies) using the charge distribution of Eq. (4). The resulting parameters were as follows:

$c = 3.7984$ fm,

$z = 0.5795$ fm,

$w = -0.1779$ fm.

This will subsequently be referred to a model 3.

The ^{40}Ca elastic form factors calculated from the three models are given in Table I. It can be seen from Table I that there is as much as 7% difference in the predictions of the form factors for the various models over the range of momentum transfers of the present experiment. Thus, it was necessary to choose between the models for the normalization of the present experiment.

Since model 2 and model 3 both reproduced the experimental energy for the mu-mesic K_α transition, the difference between these models is small. Model 3, however, is based on data taken in the same laboratory as that for model 2, but at a later time with improved techniques. Therefore, model 3 was preferred over model 2.

Model 1 does not reproduce the experimental mu-mesic K_α energy. The reason for this discrepancy may be that model 1 is based on data from Eisenstein *et al.*[16] that have been normalized to the ^{12}C elastic scattering of Engfer and Turck.[29] These ^{12}C data do not agree with the ^{12}C data of Sick and McCarthy[30] and of Jansen, Peerdeman, and de Vries.[31] If the latter two ^{12}C results are used to renormalize the data of Eisenstein, the latter are in excellent agreement with model 3. Therefore, model 3 was chosen for normalization in the present experiment.

The normalized electron scattering form factors are presented in Tables II and III. Table II gives the form factors as a function of incident electron energy, laboratory scattering angle, and momentum transfer for elastic and inelastic scattering

from ^{19}F. Table III gives the same information for inelastic electron scattering from ^{40}Ca.

ANALYSIS AND COMPARISON WITH THEORY

Elastic Electron Scattering from ^{19}F

The elastic scattering was analyzed by a phase-shift calculation using both a harmonic-oscillator charge distribution and a Fermi charge distribution. In the case of the harmonic-oscillator distribution, the variable parameter was the harmonic-oscillator length parameter, b. In the case of the Fermi charge distribution, the variable parameters were the radius parameter, c, and the skin thickness parameter, z. The results of the analysis using the normalization of model 3 are as follows:

Harmonic-oscillator distribution:

$$\langle r^2\rangle^{1/2} = 2.871 \pm 0.006 \text{ fm},$$

$$b = 1.883 \pm 0.035 \text{ fm};$$

Fermi distribution:

$$\langle r^2\rangle^{1/2} = 2.900 \pm 0.015 \text{ fm},$$

$$c = 2.592 \pm 0.045 \text{ fm},$$

$$z = 0.564 \pm 0.014 \text{ fm}.$$

These results are to be compared with the value $\langle r^2\rangle^{1/2} = 2.85 \pm 0.09$ fm derived by Backenstoss[32] from a muonic atom experiment. The value for $\langle r^2\rangle^{1/2}$ of 2.885 ± 0.015 fm adopted as the rms radius measured in this experiment was obtained by arithmetically averaging the two values above and taking the error as the larger of the two standard deviations.

Inelastic Electron Scattering from ^{19}F – Model-Independent Analysis

The form factor function for inelastic electron scattering can be written (ignoring small transverse contributions) as

$$F_L^2(q) = \frac{4\pi}{Z^2}\frac{q^{2L}}{[(2L+1)!!]^2}B(CL,q)\uparrow, \qquad (5)$$

TABLE II. Elastic and inelastic electron scattering form factors for ^{19}F.

Level	θ (deg) [a]	E (MeV) [b]	q (fm^{-1})	$F^2(q)$ Value	$F^2(q)$ standard deviation [c]
$\frac{1}{2}^+$ (g.s.)	110.75	66.02	0.550	0.4352	0.001 00
	110.75	71.02	0.592	0.3463	0.001 10
	110.64	71.03	0.591	0.3721	0.000 94
	110.64	86.05	0.716	0.219 04	0.000 53
	110.40	101.21	0.841	0.118 34	0.001 02
	110.64	101.17	0.842	0.117 90	0.000 91
	110.64	121.00	1.006	0.045 09	0.000 80
	145.82	60.88	0.589	0.3993	0.001 05
	145.79	68.55	0.663	0.2875	0.001 70
	145.82	73.94	0.715	0.2297	0.001 17
	145.70	74.45	0.720	0.2201	0.001 32
	145.40	87.96	0.849	0.112 78	0.000 89
	145.79	104.59	1.011	0.041 40	0.000 119
	145.70	104.65	1.011	0.040 98	0.000 102
	163.21	85.41	0.855	0.117 75	0.003 84
$\frac{5}{2}^+$ (0.197 MeV)	110.64	86.05	0.712	3.20×10^{-3}	0.44×10^{-3}
	110.40	101.21	0.838	3.52×10^{-3}	0.37×10^{-3}
	110.64	121.00	1.003	3.52×10^{-3}	0.34×10^{-3}
	145.82	73.94	0.711	3.52×10^{-3}	0.93×10^{-3}
	145.70	74.45	0.717	3.18×10^{-3}	1.02×10^{-3}
	145.40	87.96	0.846	3.98×10^{-3}	0.37×10^{-3}
	145.79	104.59	1.006	4.01×10^{-3}	0.36×10^{-3}
	163.21	85.41	0.851	4.28×10^{-3}	0.78×10^{-3}
$\frac{5}{2}^-$ (1.346 MeV)	110.75	66.02	0.543	1.19×10^{-4}	0.52×10^{-4}
	110.75	71.02	0.585	1.84×10^{-4}	0.45×10^{-4}
	110.64	86.05	0.709	3.97×10^{-4}	0.83×10^{-4}
	110.40	101.21	0.833	6.54×10^{-4}	0.86×10^{-4}
	110.64	121.00	0.998	10.58×10^{-4}	0.60×10^{-4}
	145.82	60.88	0.580	2.14×10^{-4}	0.80×10^{-4}
	145.82	73.94	0.705	3.91×10^{-4}	1.10×10^{-4}
	145.40	87.96	0.840	6.85×10^{-4}	0.72×10^{-4}
	145.79	104.59	1.001	9.80×10^{-4}	0.62×10^{-4}
	163.21	85.41	0.846	6.30×10^{-4}	1.92×10^{-4}
$\frac{3}{2}^+$ (1.554 MeV)	110.75	66.02	0.542	1.34×10^{-3}	0.12×10^{-3}
	110.75	71.02	0.584	1.52×10^{-3}	0.14×10^{-3}
	110.64	86.05	0.708	2.57×10^{-3}	0.11×10^{-3}
	110.40	101.21	0.832	2.76×10^{-3}	0.11×10^{-3}
	110.64	121.00	0.997	2.36×10^{-3}	0.07×10^{-3}
	145.82	60.88	0.579	1.75×10^{-3}	0.20×10^{-3}
	145.82	73.94	0.704	2.33×10^{-3}	0.27×10^{-3}
	145.50	87.96	0.839	2.85×10^{-3}	0.10×10^{-3}
	145.79	104.59	1.000	2.42×10^{-3}	0.08×10^{-3}
	163.21	85.41	0.844	3.41×10^{-3}	0.26×10^{-3}

[a] Laboratory angle.
[b] Laboratory kinetic energy.
[c] Standard deviation for statistical errors only; estimated ±2% systematic error not included.

where $B(CL,q)\uparrow$ is the reduced Coulomb longitudinal matrix element for excitation of a level from the ground state and q is the momentum transfer (MeV/c); Z is the atomic number of target nucleus; and L is the multipole order of the transition. The relationship between $B(CL,q)\uparrow$ and the reduced matrix element for decay of the state, $B(CL,q)\downarrow$, is

$$B(CL,q)\uparrow = [(2J_f+1)/(2J_0+1)]\,B(CL,q)\downarrow , \qquad (6)$$

where J_f is the spin of the excited state and J_0 is the spin of the ground state. The strength of the transition is often expressed in Weisskopf units (W.u.). If a transition proceeds with a strength of $|M^2|$ W.u., then

$$B(CL,\omega)\uparrow = \frac{|M^2|}{4\pi}\left(\frac{2J_f+1}{2J_0+1}\right)\left(\frac{3}{L+3}\right)^2 (1.2A^{1/3})^{2L} , \qquad (7)$$

where A is the atomic mass of the target.

In Born approximation the reduced matrix element may be expanded as

$$B^{1/2}(CL,q)\uparrow = B^{1/2}(CL,\omega)\uparrow \times\left[1-\frac{q^2\langle r^2\rangle_c}{2(2L+3)}+\frac{q^4\langle r^4\rangle_c}{8(2L+3)(2L+5)}\cdots\right] , \qquad (8a)$$

where

$$\langle r^l\rangle_c = \frac{\langle J_f\|\, r_{0p}^{L+l}\,\|J_0\rangle}{\langle J_f\|\, r_{0p}^{L}\,\|J_0\rangle} \qquad (8b)$$

and

$$\langle J_f\|\, r_{0p}^{L+l}\,\|J_0\rangle = \langle J_f\|\int \rho(\vec{\mathbf{r}})r^{L+l}\,Y_L(\vec{\Omega}_r)d^3\vec{\mathbf{r}}\,\|J_0\rangle . \qquad (8c)$$

At $q=\omega\approx 0$ (real photons), the longitudinal Coulomb and transverse electric matrix elements are related by Siegert's theorem

$$B(CL,\omega)\uparrow = B(EL,\omega)\uparrow . \qquad (9)$$

Thus, by using Eqs. (5) and (8a), one can extrapolate the measured form factors to $q=\omega$ and extract $B(CL,\omega)\uparrow$. From Eqs. (9) and (7) one may then obtain $B(EL,\omega)\downarrow$ [usually written as simply $B(EL)$] and $|M^2|$, the transition strength.

The expansion in Eq. (8a) is strictly valid only in plane-wave Born approximation. Appreciable error can be introduced into the determination of the transition strength if corrections are not made for distortion of the incoming and outgoing electron waves by the nuclear Coulomb field. These corrections were obtained by comparing for the Tassie[33] model a calculation of the form factors in distorted-wave Born approximation with a calculation of the form factors in plane-wave Born approximation. The experimental data were then renormalized by these correction factors. Figures 3(a) and 3(b) show the least-squares fit of Eqs. (5) and (8a) through fourth-order terms to the renormalized experimental data, and Table IV lists the parameters as determined by the fitting procedure. Figures 4(a)–4(c) display graphically the comparisons between the transition strengths measured in this experiment and by other workers. Only those measurements for which error limits are reported are given in Figs. 4(a)–4(c).

It should be pointed out that the expansion in Eq. (8a) terminated at the q^4 term is not very accurate for $q^2 \gtrsim 1$ fm^{-2}. For example, at $q^2 = 1$ fm^{-2} even the q^{10} term would contribute of the order of 7% to the sum. Thus, the value of $\langle r^4\rangle_c^{1/4}$, which depends strongly on the curvature of the function at larger q^2, would not be determined reliably by fitting Eq. (8a) to the data.

TABLE III. Inelastic electron scattering form factors for ^{40}Ca.

Level	θ (deg) [a]	E (MeV) [b]	q (fm^{-1})	$F^2(q)$ Value	$F^2(q)$ standard deviation [c]
3$^-$	110.75	71.02	0.575	8.05×10^{-4}	0.27×10^{-4}
(3.737 MeV)	110.64	86.05	0.700	1.70×10^{-3}	0.04×10^{-3}
	110.40	101.21	0.825	2.62×10^{-3}	0.04×10^{-3}
	110.64	121.00	0.990	3.27×10^{-3}	0.07×10^{-3}
	145.82	60.88	0.569	7.05×10^{-4}	0.38×10^{-4}
	145.79	68.55	0.643	1.38×10^{-3}	0.04×10^{-3}
	145.40	87.96	0.831	2.62×10^{-3}	0.05×10^{-3}
	145.79	104.59	0.992	3.12×10^{-3}	0.09×10^{-3}
2$^+$	110.75	71.02	0.575	5.43×10^{-4}	0.28×10^{-4}
(3.904 MeV)	110.64	86.05	0.700	5.29×10^{-4}	0.27×10^{-4}
	110.40	101.21	0.825	5.03×10^{-4}	0.22×10^{-4}
	110.64	121.00	0.990	2.96×10^{-4}	0.22×10^{-4}
	145.82	60.88	0.569	5.33×10^{-4}	0.37×10^{-4}
	145.79	68.55	0.643	6.56×10^{-4}	0.39×10^{-4}
	145.40	87.96	0.831	5.42×10^{-4}	0.38×10^{-4}
	145.79	104.59	0.992	2.51×10^{-4}	0.36×10^{-4}

[a] Laboratory angle.
[b] Laboratory kinetic energy.
[c] Standard deviation for statistical errors only; estimated ±2% systematic error not included.

The standard deviation of the determination in the present experiment of the transition strength for the $\frac{5}{2}^+$ (0.197-MeV) level in ^{19}F is large enough to overlap the standard deviations reported by other workers. Unfortunately, in the present experiment it was impossible to resolve this level from the strong radiation tail of the elastic peak for $q^2<0.5$ fm^{-2}. Therefore, the extrapolation to the photon point is a rather long one and is rather strongly influenced by small systematic errors. The dashed curve in Fig. 3(a) shows the least-squares fit to Eq. (8a) based only on the present experimental data.

The least-squares fit of Eq. (8a) to the inelastic scattering data for the $\frac{3}{2}^+$ (1.556-MeV) level is shown by the dot-dash curve in Fig. 3(a). In Fig. 3(a) the ordinates of all quantities relating to this

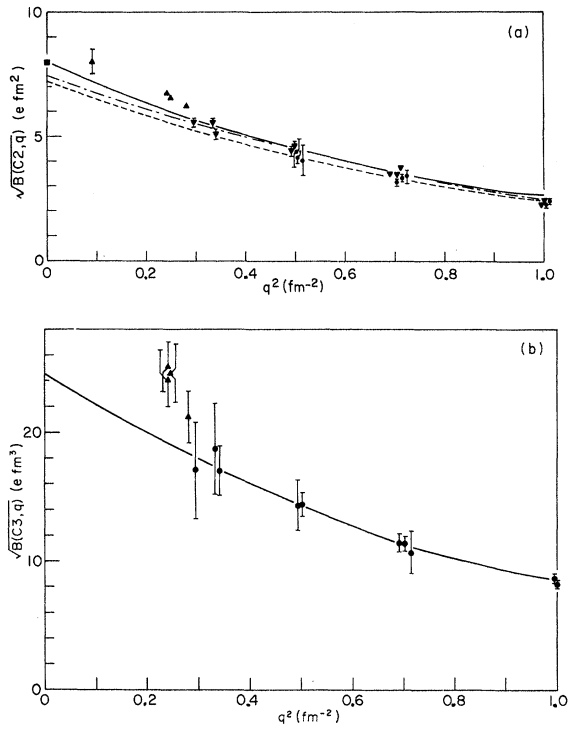

FIG. 3. Analysis of inelastic electron scattering from ^{19}F. (a) $\frac{5}{2}^+$ (0.197-MeV) and $\frac{3}{2}^+$ (1.554-MeV) levels. ●, present data, $\frac{5}{2}^+$ level. ▼, present data, $\frac{3}{2}^+$ level; ordinate scaled by $(\frac{3}{2})^{1/2}$. ▲, data of Ref. 6; ordinate scaled by $(\frac{3}{2})^{1/2}$. ■, lifetime measurement, $\frac{5}{2}^+$ level, of Ref. 2. ----, model independent fit, $\frac{5}{2}^+$ level. -·-·-, model independent fit, $\frac{3}{2}^+$ level; ordinate scaled by $(\frac{3}{2})^{1/2}$. ——, rotational model fit based on the measured ground-state charge distribution and the lifetime measurement of Ref. 2. The ordinate as given applies to the $\frac{5}{2}^+$ state. Ordinates for the $\frac{3}{2}^+$ state are obtained by multiplying the plotted ordinates by $(\frac{2}{3})^{1/2}$. (b) $\frac{5}{2}^-$ (1.346-MeV) level. ●, present data. ▲, data of Ref. 6. ——, model independent fit.

$\frac{3}{2}^+$ level have been scaled by the factor $(\frac{3}{2})^{1/2}$. The motivation for this is discussed below.

The transition strengths for the $\frac{3}{2}^+$ (1.556-MeV) level [Fig. 4(c)] as reported in Refs. 7, 1, and 6 agree with one another within their respective error estimates. The present measurement appears to be significantly smaller (about 20%) than these determinations. As can be seen in Fig. 3(a), the form factors measured in the present experiment are systematically smaller than those reported by Walcher and Strehl.[6] The source of this discrepancy is not understood. The transition strength derived for (d, d') excitation of this level is in reasonable agreement with the electromagnetic determinations within rather large error estimates.

The transition strengths for the $\frac{5}{2}^-$ (1.347-MeV) level [Fig. 4(b)] as measured by (e, e') and Coulomb-excitation experiments agree reasonably well in view of the rather large uncertainties. As seen in Fig. 3(b), the present measurements of the form factors for this level appear also to be systematically smaller (about 25%) than those measured by Walcher and Strehl.[6] The transition strengths derived for (d, d') measurements are almost an order of magnitude smaller than those derived for electromagnetic experiments and are very likely in error.

^{19}F Positive-Parity Levels

The energies and transition strengths of the low-lying positive parity levels in ^{19}F have been described by Benson and Flowers[34] as states of good angular momentum projected from a single $K=\frac{1}{2}^+$ rotational band. These authors described the nuclear surface for the intrinsic $K=\frac{1}{2}^+$ ground-state band as

$$R(\theta)=R_0[1+\beta_2 Y_{20}(\theta)+\beta_4 Y_{40}(\theta)]. \quad (10)$$

The deduced values of the quadrupole deformation parameter β_2 and the hexadecapole deformation parameter β_4 were according to Ref. 34

$$\beta_2=0.39,$$

$$\beta_4=0.17.$$

Lutz *et al.*[8] have observed the ground state and first two excited states of the positive-parity band in ^{19}F by inelastic proton scattering. On the basis of the excitation of the 4^+ member of the ground-state band in ^{20}Ne, they assign $\beta_4=\frac{1}{3}\beta_2$. Their data were analyzed in the framework of the rotational optical model in adiabatic approximation and yielded a quadrupole deformation parameter $\beta_2=0.43$. Thus, according to Ref. 8

$$\beta_2=0.43,$$

$$\beta_4=0.14.$$

TABLE IV. Transition charge parameters for ^{19}F.

Level	$B(EL, 0)\uparrow$ (e^2 fm^{2L})	$\lvert M^2\rvert$ (W.u.)	$\langle r^2_{tr}\rangle^{1/2}$ (fm)	$\langle r^4_{tr}\rangle^{1/4}$ (fm)
$\frac{5}{2}^+$ (0.197)	52^{+30}_{-24}	$5.73^{+3.30}_{-2.64}$	$3.75^{+1.08}_{-1.56}$	$3.60^{+0.79}_{-3.60}$
$\frac{5}{2}^-$ (1.346)	608^{+221}_{-187}	$9.45^{+3.43}_{-2.91}$	$4.30^{+0.88}_{-1.10}$	$4.13^{+0.68}_{-1.46}$
$\frac{3}{2}^+$ (1.554)	$35.5^{+3.9}_{-3.7}$	$5.89^{+0.65}_{-0.61}$	$3.44^{+0.29}_{-0.32}$	$2.99^{+0.37}_{-0.61}$

The data of the present experiment were analyzed by distorted-wave Born approximation using a deformed Fermi charge distribution of the form

$$\rho(r, \theta) = \rho_0 \left[1 + \exp\left((1/z)\{r - c[1 + \beta_2 Y_{20}(\theta) + \beta_4 Y_{40}(\theta)]\}\right)\right]^{-1}. \quad (11)$$

The transition charge density is then

$$\rho_{tr}(r) = 2\pi \int_0^{\pi} \rho(r, \theta) Y_{20}(\theta) \sin\theta \, d\theta . \quad (12)$$

The reduced transition matrix elements for the $K = \frac{1}{2}^+$ band are given by

$$\langle E2, q\rangle^2 = (5/16\pi)\left[q^{-2}\int_0^{\infty} \rho_{tr}(r) j_2(qr) r^2 dr\right]^2, \quad (13a)$$

$$B(E2, q; J_i \to J_f) = \langle J_i 2K0 | J_f K\rangle^2 \langle E2, q\rangle^2 . \quad (13b)$$

Equation (13b) predicts that on the basis of the rotational model the form factors for exciting the $\frac{3}{2}^+$ level should be $\frac{2}{3}$ of those for exciting the $\frac{5}{2}^+$ level. The ordinates in Fig. 3(a) have been scaled by the factor $(\frac{3}{2})^{1/2}$ for all quantities relating to the $\frac{3}{2}^+$ level. If the rotational model were valid, all the data points for the two levels would lie on a single curve. As can be seen from Fig. 3(a), this scaling holds very well, indicating that these levels are indeed well described by the rotational model.

The parameters of the charge density of Eq. (11) were determined by a variation procedure with the constraints as follows:

$$\langle r^2_{g.s.}\rangle^{1/2} = 2.885 \text{ fm},$$

$$z = 0.564 \text{ fm},$$

$$B(E2, 0)\uparrow = 63.3 \ e^2\text{fm}^4 .$$

The free variables in this calculation were the parameters of the deformed Fermi charge distribution. The form factors so calculated are indicated as the solid curve in Fig. 3(a). It is evident that the curve obtained with the rotational model for the positive-parity states in ^{19}F fits the data about as well as the model-independent calculations.

The transition radii obtained from the phase-shift calculations using the deformed rotational model are as follows:

$$\langle r^2\rangle_c^{1/2} = 4.04 \text{ fm},$$

$$\langle r^4\rangle_c^{1/4} = 4.33 \text{ fm}.$$

These values are in reasonable agreement with the transition radii obtained from the model-independent analysis (Table IV). However, the transition radii obtained from the phase-shift analysis do not suffer from the mathematical limitations mentioned above for the model-independent analysis.

In the present experiment, it was not possible to observe the transitions of multipolarity higher than $E2$ to members of the ground-state rotational band. Therefore, no direct experimental determination of the β_4 term could be made. In the analysis, two separate assumptions for β_4 were made: (i) $\beta_4 = 0$, and (ii) $\beta_4 = 0.17$ (Ref. 34). The resulting values of β_2 were as follows:

$$\beta_2 = 0.48, \qquad \beta_2 = 0.41,$$

$$\beta_4 = 0.00 \text{ (assumed)}, \qquad \beta_2 = 0.17 \text{ (Ref. 34)}.$$

This indicates that the higher-order multipoles can contribute significantly to the ground-state charge distribution. It should be noted that the β_2 measured in the present experiment agrees very well with previous determinations if the same β_4 is used.

^{19}F Negative-Parity States

The $\frac{1}{2}^-$ (0.110-MeV) and $\frac{3}{2}^-$ (1.459-MeV) states were not observed in the present experiment. The lifetime of the $\frac{1}{2}^-$ state has been measured to be $(9.2 \pm 0.4) \times 10^{-10}$ sec by Gale and Calvert.[35] This implies a dipole transition strength of about 1.5 $\times 10^{-3}$ W.u., too weak by at least 2 orders of magnitude to be observed with the sensitivity available for this experiment. The lifetime of the $\frac{3}{2}^-$ (1.459-MeV) state has been measured by Poletti, Becker, and McDonald[1] to be $(84 \pm 20) \times^{-15}$ sec. This implies a dipole transition strength of about 1.2×10^{-3} W.u., again too weak by 2 orders of magnitude to be observed in this experiment.

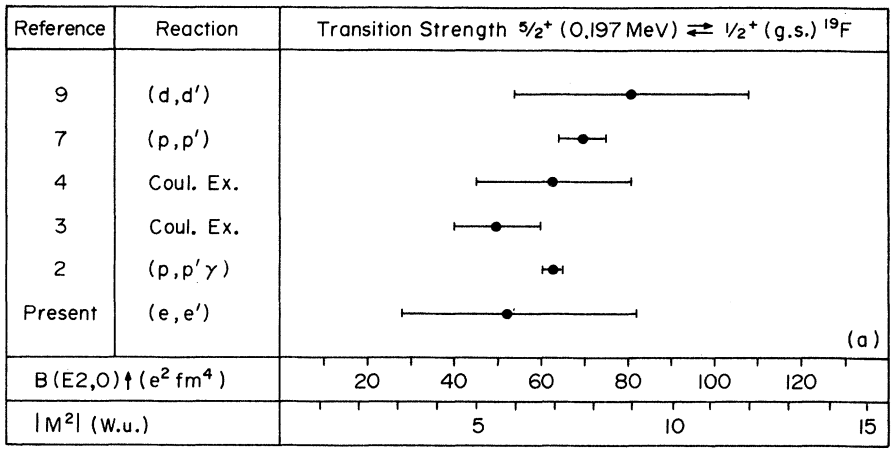

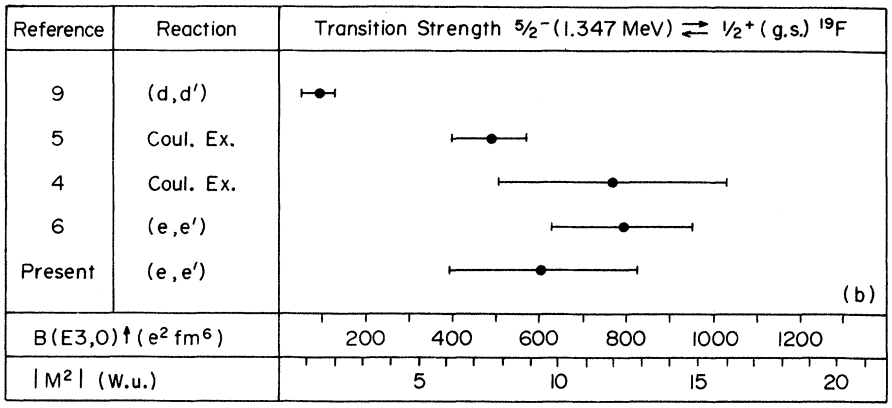

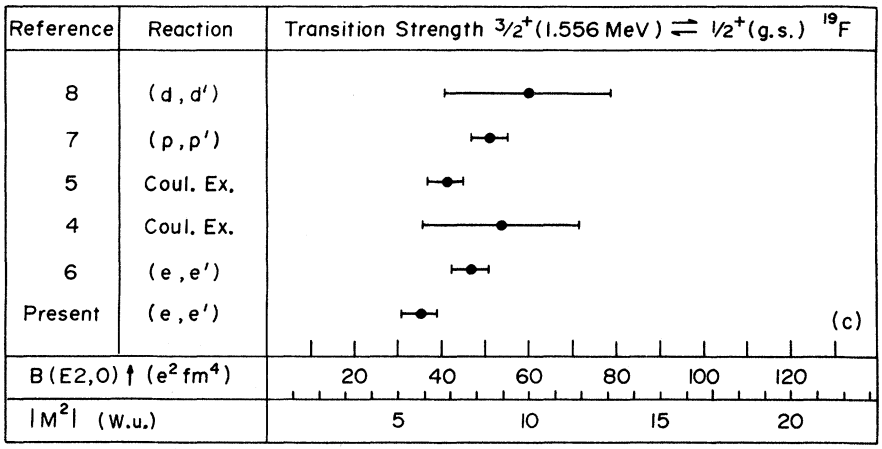

FIG. 4. Comparison of transition strengths for ^{19}F levels derived by various workers. (a) $\frac{5}{2}^+$ (0.197-MeV) level. (b) $\frac{5}{2}^-$ (1.347-MeV) level. (c) $\frac{3}{2}^+$ (1.556-MeV) level.

On the other hand, the $\frac{5}{2}^-$ level at 1.346 MeV was strongly excited in this experiment. The shape of the form factors measured for this state indicate a very small transverse part in the transition amplitude. Therefore, the principal multipole was assumed to be $E3$. The octupole transition strength measured in the present experiment was $9.45^{+3.43}_{-2.91}$ W.u.

Benson and Flowers[34] have attempted to describe the low-lying negative-parity states as a mixed band formed by coupling $p_{1/2}$ and $p_{3/2}$ proton holes to the ground-state band in ^{20}Ne. Although this model predicts the correct transition strengths for the in-band $E2$ transitions with an effective charge of $0.25e$, the prediction of the band-crossing $E3$ transition strength for the 1.346-MeV level is too small by a factor of 6 using the same effective charge.

A shell-model calculation by McGrory[36] described ^{19}F as seven particles outside a ^{12}C core. The $E3$ transition rate calculated from this model was considerably larger than that calculated from the Benson and Flowers model, but still a factor of 2 smaller than the experimental value.

The very large $E3$ transition strength suggests the possibility of octupole vibrations in ^{19}F. Phenomenological models of the octupole vibrator type have been considered by Zaikin[37] and by Krappe and Wille.[38] With these models it is possible to obtain large $E3$ transition strengths; however, it appears that at the present time there does not exist a unified model that will account for the properties of all the low-lying states in ^{19}F.

Inelastic Electron Scattering from ^{40}Ca

Calculations of the inelastic scattering form factors for ^{40}Ca were made in distorted-wave Born approximation, the electron-nucleus interaction being calculated to first order in perturbation theory. The nuclear charge and current distributions were described by a phenomenological shape modified from the vibrating liquid-drop model of Tassie.[33] The transition charge density was given by

$$\rho_{\rm tr}^{(L)}(r) = K r^{L-1} d\rho_F(r)/dr\,, \qquad (14)$$

where $\rho_F(r)$ was a two-parameter Fermi charge distribution of the form of Eq. (3). In this calculation the parameters c and z were allowed to vary in obtaining the best fit for the form factors. The resulting values of these parameters are referred to as $c_{\rm tr}$ and $z_{\rm tr}$.

The results of the calculations of the electron scattering form factors for the 3^-(3.737-MeV) level and the 2^+(3.904-MeV) level in ^{40}Ca are shown along with the experimental points in Figs. 5(a)

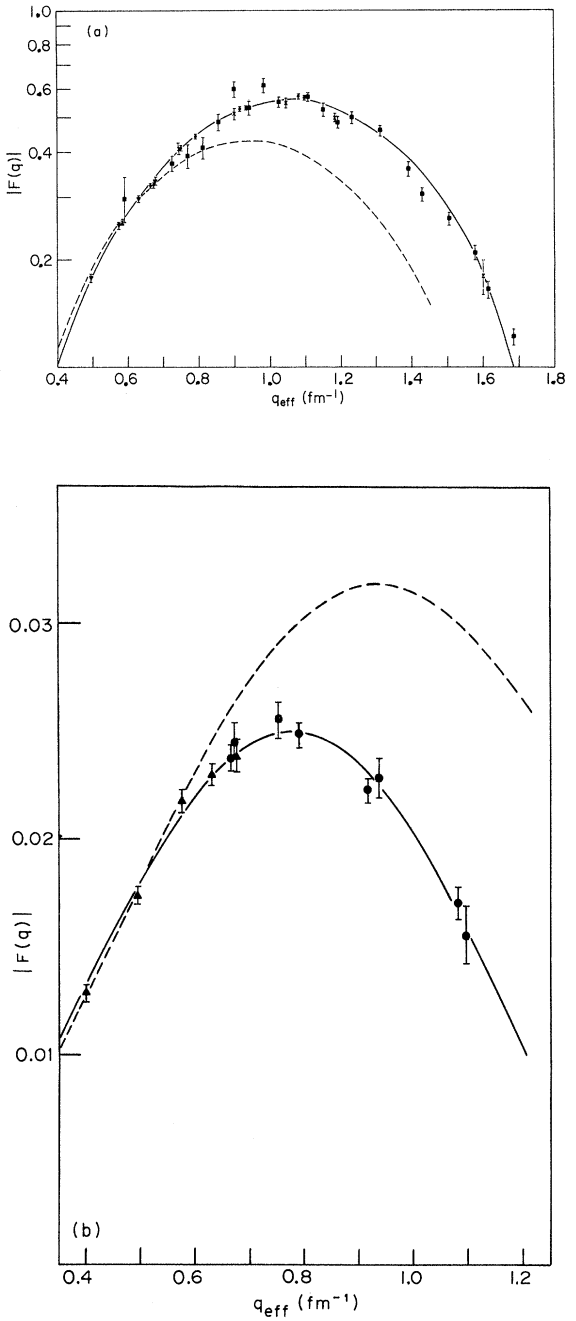

FIG. 5. Phase-shift calculation of the inelastic electron scattering form factors for ^{40}Ca using a Fermi charge distribution (model 3). (a) 3^- (3.737-MeV) level. Solid curve: Best fit form factors based on the present data plus the data of Refs. 16, 18, and 28. Dotted curve: Form factors calculated from the parameters given in Ref. 16. ●, present data. ▼, data of Ref. 16. ×, data of Ref. 18. ■, data of Ref. 28. (b) 2^+ (3.904-MeV) level. Solid curve: Best fit form factors for the present data plus the data of Ref. 16. Dotted curve: Form factors calculated from the parameters given in Ref. 16. ●, present data. ▲, data of Ref. 16.

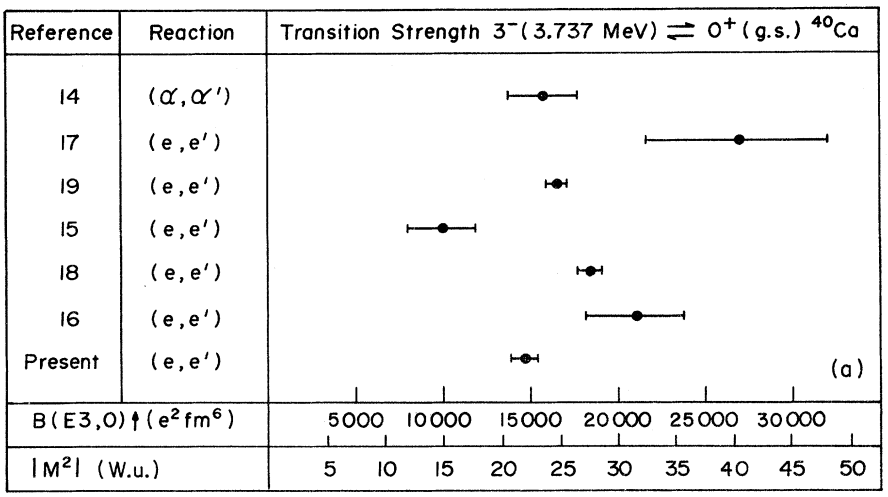

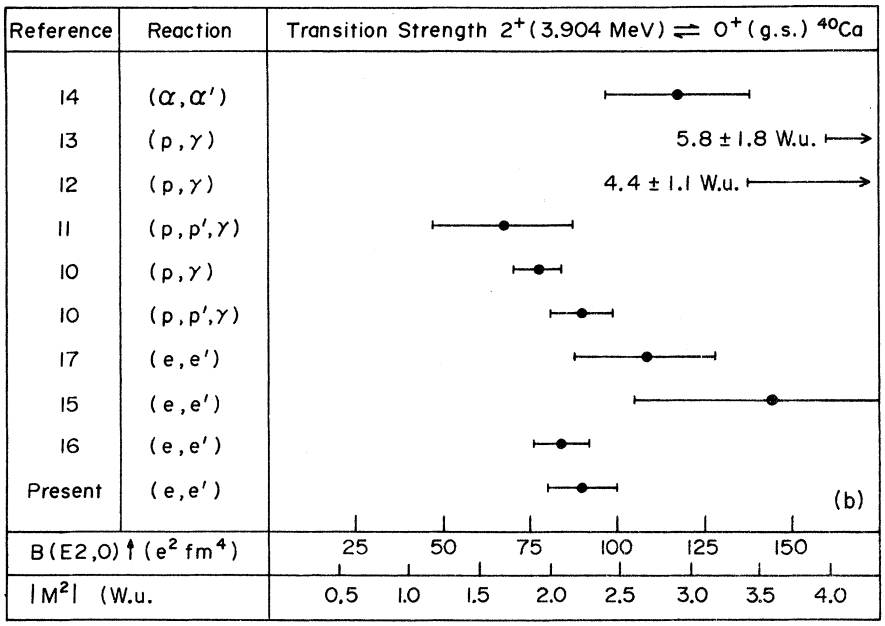

FIG. 6. Comparison of transition strengths for ^{40}Ca levels as derived by various workers. (a) 3^- (3.737-MeV) level. (b) 2^+ (3.904-MeV) level.

TABLE V. Transition charge parameters for ^{40}Ca.

Level	$B(EL,0)\uparrow (e^2\,\mathrm{fm}^{2L})$	$\lvert M^2\rvert$ (W.u.)	c_{tr} (fm)	z_{tr} (fm)	$\langle r^2_{tr}\rangle^{1/2}$ (fm)	Reference
3^- (3.737)	14870 ± 660	22.4 ± 1.0	3.534	0.430	4.80 ± 0.10	Present work
	21100 ± 2700	31.7 ± 4.0	3.712	0.524	5.68	16
2^+ (3.904)	90.2 ± 10.0	2.22 ± 0.24	3.916	0.417	4.67 ± 0.30	Present work
	84.0 ± 8.4	2.00 ± 0.20	3.212	0.457	4.38	16

and 5(b). The values of the transition strengths and transition charge parameters derived from the calculation are given in Table V. Graphical comparisons of the transition strengths measured in the present experiment to those of other workers are shown in Figs. 6(a) and 6(b).

The agreement between the present data for the transition strength for the 2^+(3.904-MeV) level of ^{40}Ca and those of previous workers is shown in Fig. 6(b). The standard deviations of the measurements of Refs. 12, 13, and 15 fail to overlap those of the present work. The agreement between the present data for the transition strength of the 3^-(3.737-MeV) level of ^{40}Ca and those of previous workers is shown in Fig. 6(a). The error limits of the present experiment overlap only those of Heisenberg, McCarthy, and Sick.[19] The determinations of Eisenstein *et al.*,[16] Itoh, Oyanada, and Torizuka,[18] and Strehl[17] are significantly larger than those of the present experiment, whereas those of Blum, Barreau, and Bellicard[15] are significantly smaller.

The difficulty of extracting $B(EL, \omega)\uparrow$ values and transition charge parameters is illustrated in Figs. 5(a) and 5(b). The solid curve in Fig. 5(a) shows the phase-shift calculations fit of the form factors for the 3^-(3.737-MeV) transition to the present data plus the data of Refs. 16, 18, and 28. Analysis of the fit yields for χ^2 of 1.58 per degree of freedom for 32 degrees of freedom. The dotted curve represents the form factors calculated from the transition parameters determined by Eisenstein *et al.*,[16] from the low-momentum-transfer data only. Figure 5(b) shows a similar comparison for the 2^+(3.904-MeV) transition. The solid curve represents the distorted-wave Born approximation form factors calculated using the present data plus the data of Ref. 16. Analysis of the fit yields χ^2 of 0.775 per degree of freedom with 10 degrees of freedom. The dotted curve represents the form factors calculated from the parameters derived by Eisenstein *et al.*[16] The least-squares analysis and evaluation of errors for the parameters were carried out as described in a previous section of this paper.

As can be seen from Figs. 5(a) and 5(b) all the data agree reasonably well within the estimated errors. The discrepancies in the transition strengths as derived by various workers appear to come from the different values of c_{tr} and z_{tr} that have been used. The fact that the quoted standard deviations for the transition strengths in many cases do not overlap indicates that the dependence of the transition strengths on c_{tr} and z_{tr} has been underestimated. These parameters in turn can be obtained with reasonable accuracy only if the form factors are measured over a range of q^2 sufficiently large to establish the curvature of the form factor function. In practical terms, this generally means that the measurements should extend from the lowest momentum transfer possible up to, and if feasible beyond, the first maximum of the form factor function.

CONCLUSIONS

^{19}F Elastic Scattering

Over the range of momentum transfers of the present experiment the elastic scattering form factors are very well described by both the harmonic-oscillator and Fermi charge distributions. The present experiment yields an rms ground-state charge radius of 2.885 ± 0.015 fm as compared to 2.85 ± 0.09 fm from muonic atom measurements.

^{19}F Inelastic Scattering

The present results for the positive-parity levels are very well explained by a rotational model in which the ground state is the leading member of a $K = \frac{1}{2}^+$ rotational band. The static quadrupole deformation parameter of the ground-state charge distribution on the basis of this model was calculated to be $\beta_2 = 0.41$ (assuming $\beta_4 = 0.17$). This is in reasonable agreement with the value $\beta_2 = 0.43$ from proton scattering results.

^{40}Ca Inelastic Scattering

The form factors for ^{40}Ca measured in the present experiment agree well with those of previous workers. However, there are serious discrepancies between the transition strengths derived from the present data and those derived by previous workers. These discrepancies seem to have their origin in the fact that the transition radius and surface thickness parameters have a much larger effect on the derived value of transition strength than has been generally appreciated. The transition charge density parameters can be reliably determined only if the form factors are measured over a wide enough range of q^2 to determine accurately the curvature of the form-factor function.

†Work supported in part by the U. S. Atomic Energy Commission, Contract No. AT(11-1)-3069.

*Present address: Physics Department, Catholic University of America, Washington, D. C.

‡Present address: U. S. Naval Postgraduate School, Monterey, California.

§Present address: Centre d'Etudes Nucleaires de Saclay, Gif-sur-Yvette, France.

[1]A. R. Poletti, J. A. Becker, and R. E. McDonald, Phys. Rev. 182, 1054 (1969).

[2]J. A. Becker, J. W. Olness, and D. H. Wilkinson, Phys. Rev. 155, 1089 (1967).

[3]P. H. Stelson and F. K. McGowan, Nucl. Phys. 16, 92 (1960).

[4]A. E. Litherland, M. A. Clark, and C. Broude, Phys. Letters 3, 204 (1963).

[5]T. K. Alexander, O. Häusser, K. W. Allen, and A. E. Litherland, Can. J. Phys. 47, 2335 (1969).

[6]T. Walcher and P. Strehl, Z. Physik 232, 342 (1970).

[7]C. M. Crawley and G. T. Garvey, Phys. Rev. 167, 1070 (1968).

[8]H. F. Lutz, J. J. Wesolowski, L. F. Hansen, and S. F. Eccles, Phys. Letters 20, 410 (1966).

[9]D. Denhard and N. M. Hintz, Phys. Rev. C 1, 460 (1970).

[10]J. R. McDonald, D. H. Wilkinson, and D. E. Alburger, Phys. Rev. C 3, 219 (1971).

[11]J. R. McDonald, D. F. H. Start, R. Anderson, A. G. Robertson, and M. A. Grace, Nucl. Phys. A108, 6 (1968).

[12]H. Lindeman, G. A. P. Engelbertink, M. W. Ockeloen, and H. S. Pruys, Nucl. Phys. A122, 373 (1968).

[13]K. W. Dolan and D. K. McDaniels, Phys. Rev. 175, 1446 (1968).

[14]A. M. Bernstein, Advan. Nucl. Phys. 3, 325 (1969).

[15]D. Blum, P. Barreau, and J. Bellicard, Phys. Letters 4, 109 (1963).

[16]R. A. Eisenstein, D. W. Madsen, H. Theissen, L. S. Cardman, and C. K. Bockelman, Phys. Rev. 188, 1815 (1969).

[17]P. Strehl, Z. Physik 234, 416 (1970).

[18]K. Itoh, M. Oyanada, and Y. Torizuka, Phys. Rev. C 2, 2181 (1970).

[19]J. Heisenberg, J. S. McCarthy, and I. Sick, Nucl. Phys. A164, 353 (1971).

[20]J. E. Leiss, Los Alamos Scientific Laboratory Report No. LA3609, 1966 (unpublished), p. 20.

[21]S. Penner, National Bureau of Standards Technical Note No. 523 (1970).

[22]J. S. Pruitt, Nucl. Instr. Methods 100, 433 (1972).

[23]J. Lightbody, Ph.D. thesis, University of Maryland, 1970 (unpublished).

[24]H. Nguyen-Ngoc and J. P. Perez-y-Jorba, Phys. Rev. 136, B1036 (1964).

[25]L. Landau, Soviet J. Phys. 8, 201 (1944).

[26]J. Schwinger, Phys. Rev. 76, 790 (1949).

[27]R. F. Frosch, R. Hofstadter, J. S. McCarthy, G. K. Noldere, K. J. van Oostrum, M. R. Yearian, B. C. Clark R. Herman, and D. G. Ravenhall, Phys. Rev. 174, 1380 (1968).

[28]J. Heisenberg, private communication.

[29]R. Engfer and D. Turck, Z. Physik 205, 90 (1967).

[30]I. Sick and J. S. McCarthy, Nucl. Phys. A150, 631 (1970).

[31]J. A. Jansen, R. Th. Peerdeman, and C. deVries, Nucl. Phys. A188, 377 (1972).

[32]G. Backenstoss, S. Charalambus, H. Daniel, H. Koch, G. Polez, H. Schmitt, and L. Tauscher, Phys. Letters 25B, 547 (1967).

[33]L. J. Tassie, Australian J. Phys. 9, 407 (1956).

[34]H. C. Benson and B. H. Flowers, Nucl. Phys. A126, 305 (1969).

[35]N. H. Gale and J. M. Calvert, Phys. Letters 7, 348 (1963).

[36]J. B. McGrory, Phys. Letters 31B, 339 (1970).

[37]D. A. Zaikin, Nucl. Phys. 86, 638 (1966).

[38]J. J. Krappe and V. Wille, Nucl. Phys. 124, 641 (1969).